A 2D microphysical analysis of aerosol nucleation in the polar winter stratosphere: implications for H_2SO_4 photolysis and nucleation mechanisms

MICHAEL J. MILLS, OWEN B. TOON
LASP, University of Colorado, Boulder

SUSAN SOLOMON
NOAA Aeronomy Laboratory, Boulder

Abstract. Each spring a layer of small particles forms between 20 and 30 km in the polar regions. Results are presented from a 2D microphysical model of sulfate aerosol, which provide the first self-consistent explanation of the observed "CN layer." Photochemical conversion of sulfuric acid to SO_2 in the upper stratosphere and mesosphere is necessary for this layer to form. Recent laboratory measurements of H_2SO_4 and SO_3 photolysis rates are consistent with such conversion, though an additional source of SO_2 may be required. Nucleation throughout the polar winter extends the top of the aerosol layer to higher altitudes, despite strong downward transport of ambient air. This finding may be important to heterogeneous chemistry at the top of the aerosol layer in polar winter and spring.

Keywords: Aerosols and particles, Middle atmosphere--composition and chemistry, Middle atmosphere--constituent transport and chemistry

Introduction

Rosen and Hofmann [1983] first noted an anomalous enhancement in springtime particle concentration near 30 km altitude at mid-latitudes in air of recent Arctic origin. Similar enhancements were observed from September to November over Antarctica [*Hofmann and Rosen*, 1985; *Hofmann*, 1988; *Hofmann et al.*, 1988; *Hofmann et al.*, 1989; *Wilson et al.*, 1989; *Hofmann*, 1990; *Hofmann and Deshler*, 1991], and in January and February over the Arctic [*Hofmann*, 1990; *Wilson et al.*, 1990]. Because the concentration is dominated by the smallest particles, known as "condensation nuclei," the polar anomaly has become known as a "CN layer."

Antarctic in situ measurements indicate modest particle nucleation at the top of the sulfate layer before the arrival of sunlight, with dramatic increases producing a well-defined layer when sunlight arrives. Balloon-borne measurements from McMurdo Station in late August 1987 and 1988 show particle concentrations increasing to a maximum of ~20 particles/cm^3 near 25 km [*Hofmann et al.*, 1989; *Hofmann*, 1990]. Because particle concentrations should otherwise decrease with air density (as is observed in polar summer), these observations suggest that nucleation occurs between 20 and 30 km in polar night. Observations made in each austral spring from 1983 to 1989 are consistent with a well-defined layer of 100-150 cm^{-3} forming each September between 22 and 28 km, with the altitude of the peak concentration descending through October to near 20-22 km in early November [*Hofmann and Rosen*, 1985; *Hofmann*, 1988; *Hofmann et al.*, 1988; *Hofmann et al.*, 1989; *Hofmann*, 1990; *Hofmann and Deshler*, 1991]. In 1993, the year following the eruption of Mt. Pinatubo, particle concentrations reached 50 cm^{-3} by late August, and peaked at about 200 cm^{-3} in early September [*Deshler et al.*, 1994].

The CN layer was first discovered in Northern Hemisphere measurements, and measurements clearly show well-defined CN events in the arctic, albeit with less consistency than the Antarctic. Observations over Kiruna, Sweden (68°N)

show a layer of 40/cm^3 between 22.5 and 26 km on January 30, 1989 [*Hofmann*, 1990]. But four profiles over Kiruna in January and February of 1992 show no definite layer, with CN concentrations constant or increasing slightly with altitude [*Deshler*, 1994]. The increasing particle mixing ratio with altitude in these profiles indicates that some nucleation occurred at the top of the layer, comparable to the weak nucleation indicated in Antarctic winter before sunrise. The variability in these arctic measurements are likely a product of the greater latitudinal excursions of vortex air in the Arctic as opposed to the Antarctic, as well as the lack of measurements well above the Arctic Circle. Trajectory analyses of the air sampled over Kiruna in 1992 indicated that it had recently been as far south as 50°N, and may have mixed with mid-latitude air. Such excursions and mixing explain the observation of the arctic CN layer over Laramie, Wyoming (41°N) in late winter and early spring of 1982, 1983, and 1986 [*Rosen and Hofmann*, 1983; *Hofmann et al.*, 1985; *Hofmann et al.*, 1988]. Because the Antarctic vortex is more circumpolar, leading to less variation in latitude and sunlit history of air parcels, and because Antarctic observations of the CN layer are more extensive and consistent than those in the Arctic, the focus of this paper is the Antarctic CN layer. It should be noted, however, that while the dynamical variability makes modeling the timing of the CN layer more complicated in the Arctic, the basic theory we present applies there as well.

Theories

Rosen and Hofmann [1983] suggested two possible origins for the CN layer. First, sulfur-bearing gases might maximize in winter, due to lack of sunlight available to oxidize them to sulfuric acid. These gases might dissociate rapidly with the return of sunlight, OH, and O in spring. Their second theory relies on very rapid drops in temperature observed in the Arctic to create very large supersaturations. In the absence of large, existing particles on which to condense, the excess of ambient vapor would nucleate many new, small particles.

Building on the nucleation rate studies of *Hamill et al.* [1990], *Zhao et al.* [1995] investigated the CN layer with a 1-dimensional microphysical model. They questioned whether sufficient sulfuric acid is present in polar winter, given the lack of photochemical production there, to initiate the temperature-dependent mechanism of *Rosen and Hofmann* [1983]. They also calculated that OCS oxidation can not provide sufficient sulfuric acid vapor to allow new particles to grow to observable size, as suggested by *Oppenheimer* [1987]. They postulated that the "extra" sulfur required for the formation of the layer can be provided by SO_2 descending from the mesosphere. The source of this SO_2 was hypothesized to be H_2SO_4 photolysis at lower latitudes. By setting upper boundary conditions of 100 pptv for both SO_2 and H_2SO_4 at 60 km and allowing for vertical subsidence, *Zhao et al.* were able to simulate the formation of a CN layer similar to that which is observed. The CN concentration was found to be much more sensitive to the SO_2 concentration than the H_2SO_4 concentration. SO_2

concentrations increase during the polar night as advection carries SO_2-rich air downward. During descent gas-phase sulfuric acid is lost on existing particles, and SO_2 remains as the dominant gaseous sulfur reservoir until the return of sunlight in spring. *Zhao et al.* did not model the production of SO_2 based on measured photolysis rates as we do here.

Photochemistry of SO_2

We present here calculations from a new microphysical model, which has been incorporated into the Garcia-Solomon two-dimensional dynamical/chemical model. The model spans 56 pressure levels from 2 to 112 km above sea level, and 36 latitude bins from 89.5°S to 89.5°N. Details of the photochemistry and dynamics of the model are described in *Garcia et al.* [1992] and *Garcia and Solomon* [1994]. We have added both sulfur oxidation chemistry and particle microphysics to this model.

OCS, tropopause SO_2, and tropopause aerosol are the sources of stratospheric aerosol in the model. Oxidation of gas-phase sulfur species is calculated according to the recommendations of *DeMore et al.* [1994] except as noted below. The mixing ratio for OCS is maintained at 510 pptv at the lower boundary of the model (750 mbar). OCS is the dominant source of sulfate at the top of the stratospheric aerosol layer. In the lower stratosphere, most of the sulfate comes from tropospheric aerosol and SO_2, which are maintained at constant mixing ratios of 0.27 ppbm of $SO_4^=$ and 80 pptv of SO_2 at the model's tropical tropopause. Tropospheric aerosol is represented by a bimodal lognormal distribution, with 30% of the mass in a 0.8-μm radius mode, and the majority of particles distributed about 0.015μm. The details of these tropospheric sources of sulfur do not affect the calculation of the polar CN layer.

As temperatures increase with altitude in the stratosphere, sulfate aerosol evaporates, producing sulfuric acid vapor. This vapor is thought to photolyze to SO_2 at the short wavelengths of sunlight present in the upper stratosphere and mesosphere. *Rinsland et al.* [1995] concluded from observations of SO_2 in the upper stratosphere and mesosphere and from 2-dimensional model calculations, that sulfuric acid vapor should photolyze at rates roughly 0.3 times that of HCl. We present this assumption as model case A (see table 1). Recently, *Burkholder et al.* [1998] measured no photolytic cross sections for H_2SO_4 vapor greater than their upper limit of 10^{-21} cm^2, for wavelengths greater than 195 nm. Our model case B sets the cross sections to that upper limit of 10^{-21} cm^2 in the 179-226 nm region where HCl absorbs, representing maximum photolysis rates consistent with the findings of *Burkholder et al.* Case C assumes that the cross section is 10^{-21} cm^2 at 195 nm, with the same wavelength dependence as HCl (decreasing with increasing wavelength). This assumption sets the cross sections to 0.011 times those of HCl. Case D assumes that H_2SO_4 vapor does not photolyze at all.

Burkholder and McKeen [1997] recently measured SO_3 photolysis cross sections, which we have included in the model. This reaction is an important source of SO_2 near the top of the sulfate layer, where SO_3 photolyzes faster than it oxidizes to H_2SO_4. The oxidation of SO_3 proceeds through the production of an $SO_3 \bullet H_2O$ adduct, resulting in a pressure-dependent effective reaction rate [*Lovejoy et al.*, 1996]. The timescale for oxidation increases exponentially with altitude, from a few seconds near the tropopause to a few days at 40 km. Photolysis becomes faster with altitude, overtaking oxidation as the dominant loss for SO_3 near 40 km. Model cases A through D include SO_3 photolysis. We test the importance of the new SO_3 photolysis reaction to the formation of the CN layer with case E and F, which are the same as cases B and D, respectively, but without SO_3 photolysis.

Calculated SO_2 mixing ratios for cases B, D, E, and F are shown in Figure 1, revealing the effects of photolysis of H_2SO_4, SO_3, and SO_2. The figures show SO_2 on June 1 building up to more than 170 pptv in case B. Mixing ratios are greatest in polar winter, where destruction by photolysis is shut off, and SO thus formed reverts to SO_2.

Particle Microphysics

The microphysical model includes classical binary homogeneous nucleation; coagulation; condensation and evaporation of water, sulfuric acid, and nitric acid; transport with ambient air parcels; and sedimentation [*Mills*, 1996]. The model simulates the formation of Type Ib (liquid ternary solutions) and Type II (water ice) polar stratospheric clouds, but does not deal with Type Ia (nitric acid hydrate) PSCs. Aerosol particles are divided into 45 size classes ranging from ~0.5 nm to ~10 μm.

Calculation of binary homogeneous nucleation rates is highly uncertain. *Wyslouzil et al.* [1991] present laboratory measurements of nucleation rates, showing discrepancies of ±10 orders of magnitude with classical theory. *Weber et al.* [1996] conclude from atmospheric measurements that particle number varies as the square of sulfuric acid concentrations, rather than the classically predicted exponential response. *Brock et al.* [1995] point out, however, that despite these uncertainties, classical nucleation theory correctly predicts the regions in the atmosphere in which large numbers of particles are observed. After experimenting with alternative nucleation parameterizations based on the findings of *Wyslouzil et al.* and *Weber et al.*, we conclude that classical nucleation theory provides the best correspondence with observed aerosol behavior in the stratosphere.

Figure 2 shows the calculated concentrations of particles larger than 0.01 μm, the lower size limit of balloon-borne CN counters, from the 6 model cases described in Table 1. Cases A and B reproduce well the observed particle concentrations in both winter and spring. In these cases, particle production is evident throughout the winter, with dramatic

increases to 80-120 particles/cm^3 in September. The CN layer descends from 30 to 22 km as the austral spring progresses. Measurements made repeatedly in the spring of a given year show the CN layer to be descending in a similar manner [*Hofmann et al.*, 1988; *Hofmann et al.*, 1989; *Deshler et al.*, 1994]. Although the observed CN layer sometimes initiates as low as 26 km, these observations also indicate the presence of enhanced CN concentrations at 30 km. The calculations diverge from observations in the other model cases, when either H_2SO_4 or SO_3 photolysis rates are decreased.

Figure 3 shows the seasonal cycle of temperature, nucleation, and particle concentration for case B. There is a small, but significant rate of nucleation near 30 km as early as April which continues throughout the winter, as cold temperatures (below 220 K) reach higher altitudes. Prior to July, at any given altitude nucleation returns to negligible rates within several weeks of its initiation, despite continued decreases in temperature, as aerosol formation and growth deplete ambient sulfuric acid vapor. The winter phase of nucleation produces small concentrations (10-50 /cm^3) of particles, most of which grow to observable size at the 30 km maximum. Observations at McMurdo Station (78°S) show particle concentrations increasing slightly from about 10 /cm^3 at 16 km to about 20/cm^3 at 26 km in late August, before the well-defined CN layer forms [*Hofmann et al.*, 1989; *Hofmann*, 1990]. Our calculations suggest similar concentrations of observable particles at 26 km. Aerosol is not suppressed by the strong descent prevalent in polar winter, but instead is present at higher altitudes than in summer due to nucleation. If the only source of particles were at lower altitudes (i.e. the tropopause), subsidence would push down the top of the layer in polar stratospheric winter.

About a month after temperatures reach their minimum below 190K in late June and early July, particle nucleation increases dramatically at all altitudes below about 36 km. Particle concentrations respond rapidly, peaking at over 10^4/cm^3 between 22 and 30 km. This event coincides with the return of sunlight in late July, and continues until temperatures increase to greater than 200 K at the beginning of October. A layer of observable-sized particles forms above 30 km in early September, descending in altitude and increasing in concentration until a maximum of about 80/cm^3 is found near 26 km in late October. This maximum in observable particles occurs nearly 2 months after the peak in total particle concentration.

The delay between the minimum in temperature and the maximum in calculated nucleation, and the subsequent lag between concentrations of total particles and observable particles depend critically on the descent of SO_2 from above. Figure 4 shows the annual cycles of various calculated gas-phase species and aerosol parameters at 26 km and 74°S for cases B, D, and E. The arrival of polar night at 74°S is evident from the dramatic drop in OH as photolytic production shuts off at the end of May. Air descends from the mesosphere to the stratosphere throughout polar winter. In case B, the air carries with it mixing ratios of SO_2 as high as 160 pptv at some altitudes (see Figure 1). Liquid sulfate mass, shown in Figure 4, decreases by sedimentation and descent throughout the austral winter in all three cases.

In mid-May, the disappearance of OH cuts off all production of H_2SO_4 vapor, while the rate of loss due to condensation increases slightly on newly nucleated particles descending from above 30 km (see Figure 3). Loss of production and enhancement of the sink causes H_2SO_4 mixing ratios to plummet by 2-4 orders of magnitude in cases B, D, and E. The effect is greatest in case D because more H_2SO_4 vapor is available for nucleation above 30 km in May, resulting in greater surface areas and faster condensation.

Sulfuric acid vapor recovers in July, coincident with the return of sunlight and OH. At that time production of H_2SO_4 vapor from SO_2 resumes (quite rapidly in cases B and E) as SO_2 has increased to more than 50 times its summertime minimum. The increase in sulfuric acid vapor concentration by two orders of magnitude in July, while cold temperatures continue to suppress equilibrium vapor pressures, generates significant nucleation rates, especially in cases B and E. Sustained over the months of August and September, the nucleation event produces particle concentrations in excess of 10^4 /cm^3 in these cases (see Figure 3).

By late September these particles at 26 km grow to observable size in case B. The growth in particle size coincides with a dramatic increase in liquid sulfate mass, indicating that this growth is not due merely to coagulation. The steady increase in OH with increasing sunlight as spring progresses hastens the conversion of SO_2 to sulfuric acid, which condenses on the recently nucleated particles, rather than nucleating new ones. Nucleation shuts off in early October in favor of condensation due to rising temperatures. At 26 km in polar winter, homogeneous nucleation rates calculated from classical theory decrease by about 6 orders of magnitude as temperature increases from 180K in late September to 200K in early October. Condensation rates have a much lesser dependence on temperature.

Comparison of cases B, D, and E in Figure 4 reveals the importance of both SO_3 and H_2SO_4 photolysis to the production of a CN layer resembling that observed. H_2SO_4 photolysis provides an essential mechanism for suppressing homogeneous nucleation in winter and conserving gas-phase sulfur as SO_2, which becomes available again as H_2SO_4 in the spring to fuel nucleation. Although *Burkholder et al.*'s measurements reveal no evidence for H_2SO_4 photolysis, their upper limit produces enough SO_2, in conjunction with SO_3 photolysis, to create a CN layer similar to that observed. SO_3 photolysis prevents SO_2 from oxidizing back to H_2SO_4. At 40 km SO_3 photolysis can increase descending SO_2 mixing ratios by 50 pptv (see Figure 1), and at 26 km it increases the peak SO_2 mixing ratio seen in September by a factor of 2.25 (see Figure 4).

Figure 5 shows the effect of the CN layer on aerosol surface areas at 74°S in each of the six model cases. In all cases, surface areas between 30 and 35 km are enhanced in the winter and spring relative to summer and autumn. H_2SO_4 photolysis in cases A and B results in springtime surface areas enhanced by as much as a factor of 2 over cases D and F, in which H_2SO_4 photolysis is turned off. Polar winter nucleation and the springtime CN layer may affect heterogeneous

reactions between sulfate aerosol and various gas-phase species on a seasonal basis. In all cases, surface areas of 0.1 $\mu m^2/cm^3$ or greater extend up to 36 km throughout winter and spring, and to less than 30 km in summer and autumn. Depending on reaction probabilities and ambient concentrations of gas-phase species, such surface areas could perturb gas-phase species via heterogeneous chemistry. In the absence of new particle nucleation above 30 km, dynamical descent in the polar winter would suppress the sulfate aerosol layer, reducing rather than increasing the altitude of the top of the layer relative to summer.

Conclusions

The 2D microphysical model of sulfate aerosol that we have developed provides the first self-consistent explanation of the CN layer observed in Antarctic spring. Although dynamics complicate the Arctic situation, the same theory applies to enhanced CN observed there [*Hofmann*, 1990; *Wilson et al.*, 1990; *Deshler*, 1994].

Binary homogeneous nucleation and condensation following rapid production of sulfuric acid vapor from SO_2 in spring is responsible for the appearance of a CN layer, as suggested by *Zhao et al.* [1995]. Photolysis of SO_3 and H_2SO_4 are proposed as the mechanism for producing SO_2 in the upper stratosphere and mesosphere; downward transport in polar winter and spring then bring the SO_2 into the lower stratosphere. The model demonstrates that photolysis of SO_3 and H_2SO_4, calculated within the constraints of recent laboratory measurements, can partition sulfur as SO_2 in the upper stratosphere and mesosphere to produce a springtime CN layer much like that observed. However, when a wavelength dependence in the H_2SO_4 cross sections matching that of HCl further constrains photolysis, the calculated CN layer has substantially smaller concentrations than that observed. An additional source for SO_2 in the upper stratosphere and mesosphere may be indicated to explain the CN layer, as well as observations of SO_2 at these altitudes.

The model also suggests that new particles nucleate and grow throughout the winter above 30 km, at a slower rate than that which produces springtime CN layer. Thus aerosol is present at higher altitudes in polar winter than in summer, despite the subsidence of polar air which would otherwise push the top of the aerosol layer downward. Concentrations of new particles thus formed are consistent with *in situ* measurements made in polar winter. These particles may be important to heterogeneous chemistry at the top of the aerosol layer in polar winter and spring.

Aknowledgments. This work was supported in part by the NASA SAGE II Science Team through grant L68687D and NASA's Atmospheric Chemistry Program NAG1-2021.

Tables

Case	H_2SO_4 cross sections		SO_3 photolysis
A	$\sigma_{H2SO4}=0.3\bullet\sigma_{HCl}$	Rinsland fit to observations	On
B	$\sigma_{H2SO4}=10^{-21}$ cm^2	*Burkholder et al.* upper limit	On
C	$\sigma_{H2SO4}=0.011\bullet\sigma_{HCl}$	Upper limit with HCl tail	On
D	$\sigma_{H2SO4}=0.0$	No H_2SO_4 photolysis	On
E	$\sigma_{H2SO4}=10^{-21}$ cm^2	*Burkholder et al.* upper limit	Off
F	$\sigma_{H2SO4}=0.0$	No H_2SO_4 photolysis	Off

Table 1. Model cases, varying H_2SO_4 and SO_3 photolysis.

Figure Captions

Figure 1. SO_2 mixing ratios (pptv) for four model cases representing various assumptions about H_2SO_4 and SO_3 photolysis. Calculations are shown for noon, June1.

Figure 2. Calculated concentrations (/cm^3) of particles large enough to be observed (r>0.01μm) in six model cases, varying photolysis rates for H_2SO_4 and SO_3. Results are presented as annual cycles at 74°S, averaged over 5-day periods for each altitude gridpoint (2 km resolution). In cases A and B, CN layers are calculated which resemble those observed. SO_3 photolysis is included in cases A through D. Comparison of cases B and E reveals the importance of SO_3 photolysis to the concentration of particles in the CN layer.

Figure 3. Model calculations of (a) temperatures, (b) homogeneous binary nucleation rates, (c) total particle concentrations, and (d) particles of radius greater than 0.01μm at 74°S in model case B. A delay of about one month is evident between the periods of minimum temperature and maximum nucleation. A similar delay occurs between the maximum in total particle concentration and that in particles large enough to be observed.

Figure 4. Variation in OH, SO2, sulfate mass, aerosol surface area, sulfuric acid vapor, sulfuric acid equilibrium vapor pressure, nucleation rate, and particles greater than 0.01 micron radius at 26 km, 74°S for model cases B, D, and E (see table 1 and text).

Figure 5. Calculated CN layer surface areas (μm^2/cm^3) in six model cases at 74°S.

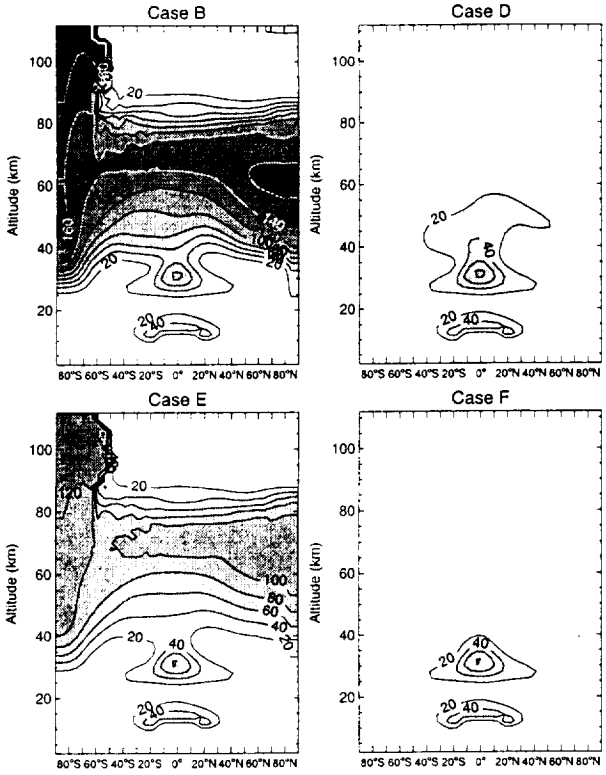

Figure 1

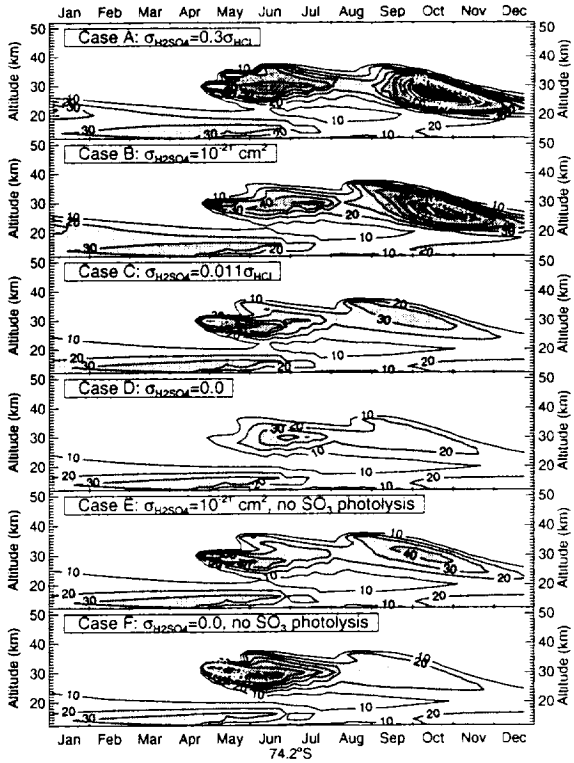

Figure 2

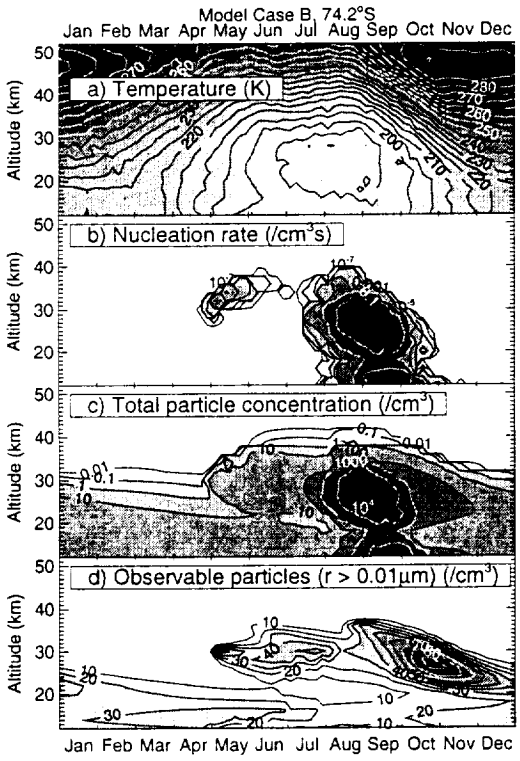

Figure 3

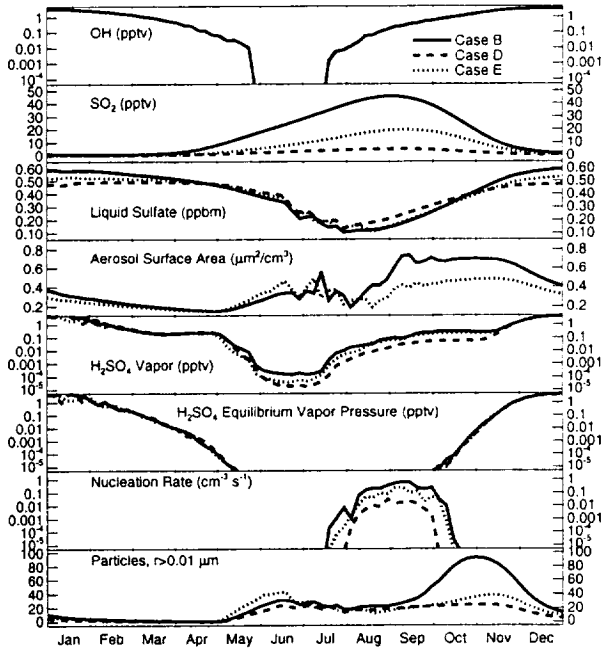

Figure 4

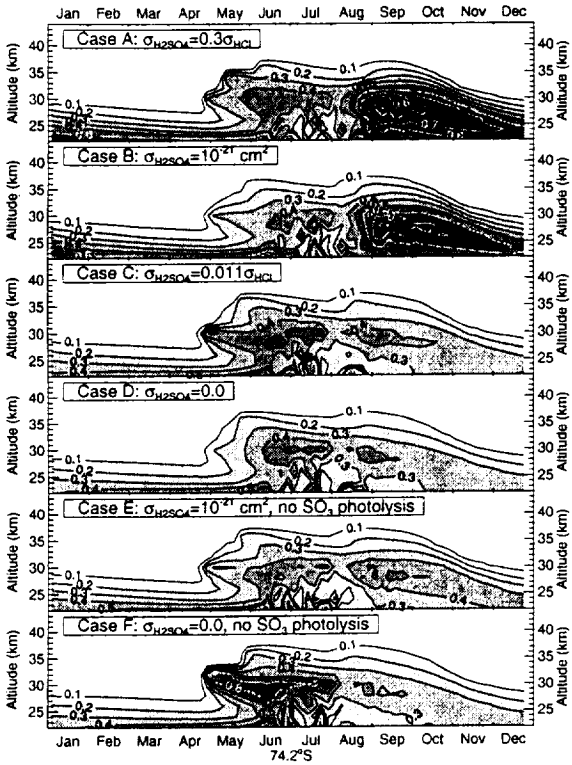
Jan Feb Mar Apr May Jun Jul Aug Sep Oct Nov Dec
Case A: $\sigma_{H2SO4}=0.3\sigma_{HCl}$
Case B: $\sigma_{H2SO4}=10^{-21}$ cm^2
Case C: $\sigma_{H2SO4}=0.011\sigma_{HCl}$
Case D: $\sigma_{H2SO4}=0.0$
Case E: $\sigma_{H2SO4}=10^{-21}$ cm^2, no SO_3 photolysis
Case F: $\sigma_{H2SO4}=0.0$, no SO_3 photolysis
Altitude (km)
74.2°S

Figure 5

References

Brock, C.A., P. Hamill, J.C. Wilson, H.H. Jonsson, and K.R. Chan, Particle formation in the upper tropical troposphere: a source of nuclei for the stratospheric aerosol, *Science, 270*, 1650-1653, 1995.

Burkholder, J., S. McKeen, and M. Mills, Upper limit for the UV absorption cross-sections of H_2SO_4, *Geophysical Research Letters, to be submitted*, 1999.

Burkholder, J.B., and S. McKeen, UV absorption cross sections for SO_3, *Geophysical Research Letters, 24* (24), 3201-3204, 1997.

DeMore, W.B., S.P. Sander, D.M. Golden, R.F. Hampson, M.J. Kurylo, C.J. Howard, A.R. Ravishankara, C.E. Kolb, and M.J. Molina, Chemical Kinetics and Photochemical Data for Use in Stratospheric Modeling, Jet Propulsion Laboratory, 1994.

Deshler, T., In situ measurements of Pinatubo aerosol over Kiruna on four days between 18 January and 13 February 1992, *Geophysical Research Letters, 21* (13), 1323-1326, 1994.

Deshler, T., B.J. Johnson, and W.R. Rozier, Changes in the character of polar stratospheric clouds over Antarctica in 1992 due to the Pinatubo volcanic aerosol, *Geophysical Research Letters, 21* (4), 273-276, 1994.

Garcia, R.R., and S. Solomon, A new numerical model of the middle atmosphere 2. Ozone and related species, *Journal of Geophysical Research, 99* (D6), 12,937-12,951, 1994.

Garcia, R.R., F. Stordal, S. Solomon, and J.T. Kiehl, A new numerical model of the middle atmosphere 1. Dynamics and transport of tropospheric gases, *Journal of Geophysical Research, 97*, 12,967-12,991, 1992.

Hamill, P., O.B. Toon, and R.P. Turco, Aerosol nucleation in the winter Arctic and Antarctic stratosphere, *Geophysical Research Letters, 17*, 417-420, 1990.

Hofmann, D.J., Balloon-borne measurements of middle atmosphere aerosol and trace gases in Antarctica, *Reviews of Geophysics, 26*, 113-130, 1988.

Hofmann, D.J., Measurement of the condensation nuclei profile to 31 km in the Arctic in January 1989 and comparisons with Antarctic measurements, *Geophysical Research Letters, 17* (4), 357-360, 1990.

Hofmann, D.J., and T. Deshler, Stratospheric cloud observations during formation of the Antarctic ozone hole in 1989, *Journal of Geophysical Research, 96* (D2), 2897-2912, 1991.

Hofmann, D.J., and J.M. Rosen, Antarctic observations of stratospheric aerosol and high altitude condensation nuclei following the El Chichon Eruption, *Geophysical Research Letters, 12* (1), 13-16, 1985.

Hofmann, D.J., J.M. Rosen, and W. Gringel, Delayed production of sulfuric acid condensation nuclei in the polar stratosphere from El Chichon volcanic aerosols, *Journal of Geophysical Research, 90* (2), 2341-2354, 1985.

Hofmann, D.J., J.M. Rosen, and J.W. Harder, Aerosol measurements in the winter/spring Antarctic stratosphere. 1. Correlative measurements with ozone, *Journal of Geophysical Research, D93* (1), 665, 1988.

Hofmann, D.J., J.M. Rosen, J.W. Harder, and J.V. Hereford, Balloon-borne measurements of aerosol, condensation nuclei, and cloud particles in the stratosphere at McMurdo Station, Antarctica, during the spring of 1987, *Journal of Geophysical Research, D94* (9), 11,253-11,269, 1989.

Lovejoy, E.R., D.R. Hanson, and L.G. Huey, Kinetics and products of the gas-phase reaction of SO_3 with water, *Journal of the American Chemical Society*, 1996.

Mills, M.J., Stratospheric Sulfate Aerosol: A Microphysical Model, Ph.D. thesis, University of Colorado, 1996.

Oppenheimer, M., A photochemical source for condensation nuclei in the Antarctic circumpolar vortex, *Nature*, *328*, 702-704, 1987.

Rinsland, C.P., M.R. Gunson, M.K.W. Ko, D.W. Weisensten, R. Zander, M.C. Abrams, A. Goldman, N.D. Sze, and G.K. Yue, H_2SO_4 photolysis: A source of sulfur dioxide in the upper stratosphere, *Geophysical Research Letters*, *22* (9), 1109-1112, 1995.

Rosen, J.M., and D.J. Hofmann, Unusual behavior in the condensation nuclei concentration at 30 km, *Journal of Geophysical Research*, *88* (C6), 3725-3731, 1983.

Weber, R.J., J.J. Marti, P.H. McMurry, F.L. Eisele, D.J. Tanner, and A. Jefferson, Measured atmospheric new particle formation rates: implications for nucleation mechanisms, *Chemical engineering communications*, *151*, 53-64, 1996.

Wilson, J.C., M. Loewenstein, D.W. Fahey, B. Gary, S.D. Smith, K.K. Kelly, G.V. Ferry, and K.R. Chan, Observations of condensation nuclei in the Airborne Antarctic Ozone Experiment: Implications for new particle formation and polar stratospheric cloud formation, *Journal of Geophysical Research*, *94* (D14), 16,437-16,448, 1989.

Wilson, J.C., M.R. Stolzenburg, W.E. Clark, M. Loewenstein, G.V. Ferry, and K.R. Chan, Measurements of condensation nuclei in the airborne Arctic stratospheric expedition: Observations of particle production in the polar vortex, *Geophysical Research Letters*, *17* (4), 361-364, 1990.

Wyslouzil, B.E., J.H. Seinfeld, R.C. Flagan, and K. Okuyama, Binary nucleation in acid-water systems. II. Sulfuric acid-water and a comparison with methanesulfonic acid-water, *Journal of Chemical Physics*, *94* (10), 6842-6850, 1991.

Zhao, J.X., O.B. Toon, and R.P. Turco, Origin of condensation nuclei in the springtime polar stratosphere, *Journal of Geophysical Research*, *100* (D3), 5215-5227, 1995.